

# Diffusion Models are Efficient Data Generators for Human Mesh Recovery

Yongtao Ge, Wenjia Wang, Yongfan Chen, Fanzhou Wang, Lei Yang, Hao Chen, Chunhua Shen

**Abstract**—Despite remarkable progress having been made on the problem of 3D human pose and shape estimation (HPS), current state-of-the-art methods rely heavily on either confined indoor mocap datasets or datasets generated by a rendering engine using computer graphics (CG). Both categories of datasets exhibit inadequacies in furnishing adequate human identities and authentic in-the-wild background scenes, which are crucial for accurately simulating real-world distributions. In this work, we show that synthetic data created by generative models is complementary to CG-rendered data for achieving remarkable generalization performance on diverse real-world scenes. We propose an effective data generation pipeline based on recent diffusion models, termed **HumanWild**, which can effortlessly generate human images and corresponding 3D mesh annotations. Specifically, we first collect a large-scale human-centric dataset with comprehensive annotations, *e.g.*, text captions, the depth map, and surface normal images. To generate a wide variety of human images with initial labels, we train a customized, multi-condition ControlNet model. The key to this process is using a 3D parametric model, *e.g.*, SMPL-X, to easily create precise 2D keypoints, depth maps, and surface normal images by rendering the 3D mesh with specific camera parameters. As there exists inevitable noise in the initial labels, we apply an off-the-shelf foundation segmentation model to filter negative data samples, and a 2D vertex estimator to rectify the SMPL-X parameters by using SMPLify. Our data generation pipeline is both flexible and customizable, making it adaptable to various real-world tasks, such as human interaction in complex scenes and humans captured by wide-angle lenses. By relying solely on generative models, we can produce large-scale, in-the-wild human images with high-quality annotations, significantly reducing the need for manual image collection and annotation. The generated dataset encompasses a wide range of viewpoints, environments, and human identities, ensuring its versatility across different scenarios. To verify the effectiveness of the generated data, we perform comprehensive data ablation experiments by performing data ablation studies on top of the both generated data and existing datasets, and evaluating on a wide range of HPS benchmarks. We hope that our work could pave the way for scaling up 3D human recovery to in-the-wild scenes.

**Index Terms**—Controllable Human Generation, Synthetic Dataset, Human Pose and Shape Estimation, Diffusion Models

## 1 INTRODUCTION

Estimating human pose and shape (HPS) [1], [2], [3], [4], [5] from a single RGB image is a core challenge in computer vision and has many applications in robotics [6], [7], [8], computer graphics [9], [10], and digital content creation [11]. Current HPS estimation methods require well-annotated datasets to achieve good performance. Unfortunately, collecting large-scale, versatile 3D human body data is time-consuming and expensive.

Contemporary methodologies for acquiring precise 3D human body data predominantly employ two primary pipelines. The first pipeline involves indoor motion capture (mocap) systems, including both marker-based and vision-based approaches, which are employed by many existing datasets [12], [13], [14], [15] to capture human body attributes. However, this mocap pipeline faces two primary limitations. First, mocap systems are intricate and costly, and their complex operation demands specialized expertise. Second,

the data captured is not very diverse. Datasets usually feature a limited number of actors in a lab or studio, which restricts the collection of large-scale human data in more varied environments. To diversify the data sources, some researchers also capture 3D pseudo ground truth by estimating from 2D clues or using additional sensors. SMPLify [16] proposed to fit the parameters of a 3D human model to the location of 2D keypoints. EFT [17] introduced the Exemplar Fine-Tuning strategy by overfitting a pre-trained 3D pose regressor with 2D keypoint reprojection loss, taking the final output of the regressor as pseudo labels. However, these methodologies face challenges in accurately generating camera parameters and body parameters, leading to sub-optimal performance on in-the-wild 3D human pose and shape estimation.

An alternative approach is to generate 3D human datasets using computer-generated (CG) rendering, as seen in works like GTA-Human [18], BEDLAM [19] and SynBody [20]. However, this method has two main challenges. First, there are significant costs involved in obtaining high-quality 3D assets, such as avatars and scene elements, as well as the need for specialized skills in 3D rendering. Second, making synthetic humans and backgrounds look realistic is a major hurdle. There’s often a noticeable visual difference between the rendered images and real-world photographs. While Black et al. [19] show the potential of high-quality synthetic data to replace real images, they also highlight important limitations. Their work demonstrates that CLIFF [4], when trained only on synthetic data, can outperform

- Accepted to IEEE Trans. Pattern Analysis and Machine Intelligence, Oct. 2025. This version includes the supplementary material, and can be slightly different from the final version.
- Yongtao Ge is with The University of Adelaide. This work was done when he was visiting Zhejiang University.
- Chunhua Shen is with Zhejiang University of Technology.
- Yongtao Ge, Yongfan Chen, Hao Chen, and Chunhua Shen are with Zhejiang University.
- Wenjia Wang is with The University of Hong Kong.
- Fanzhou Wang and Lei Yang are with SenseTime.
- The corresponding author is Chunhua Shen: chunhuashen@zju.edu.cn

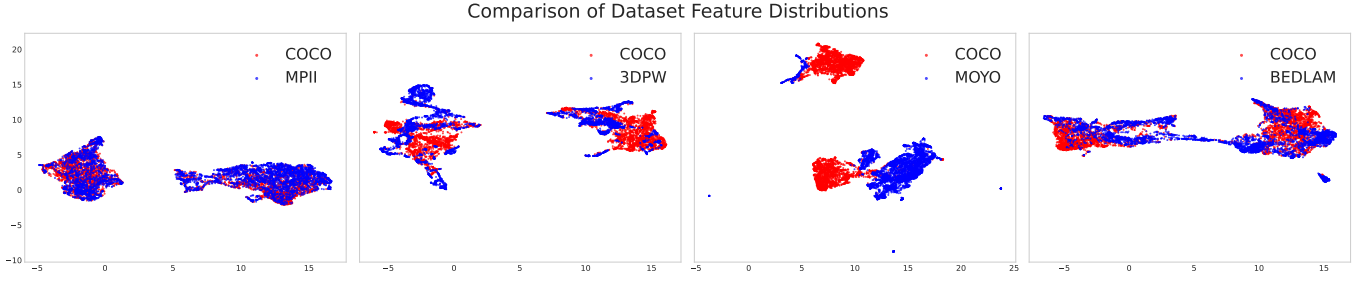


Fig. 1: Dataset appearance distributions of synthesized datasets and in-the-wild real-world datasets.

models trained on real datasets. Conversely, they report that training HPS models from scratch with synthetic data, without leveraging pre-training on real-world 2D keypoints datasets (like COCO [21]), leads to inferior results. The study further reveals the significant positive impact of realistic clothing simulation compared to more basic textured bodies. This suggests that while synthetic data is a powerful tool, the degree of realism in the data is crucial for advancing 3D human pose and shape estimation.

While 2D keypoint detectors generalize well when trained on large in-the-wild datasets like COCO, significant gaps exist with 3D datasets. To investigate these gaps, we visualized the feature distributions of several key datasets. We extracted features from cropped human images using DINO-v2 and used UMAP for dimensionality reduction, as shown in Fig. 1. Our analysis compares the real-world 2D datasets COCO [21] and MPII [22] against three distinct 3D datasets: the real-world outdoor 3DPW [23], the indoor Mocap MOYO [13], and the synthetically rendered BEDLAM [19]. The visualization reveals three key insights: (1). The feature distributions of the two real-world 2D datasets, COCO and MPII, are nearly identical. (2). In contrast, both the outdoor 3DPW and indoor MOYO datasets show distributions that diverge significantly from COCO. (3). The CG-rendered BEDLAM dataset is closer to COCO’s distribution than the other 3D datasets, though a noticeable gap remains.

This work introduces an automatic and scalable pipeline for generating synthetic data for 3D human pose and shape estimation. Our method uses generative models to create data with more realistic human distributions, overcoming a key limitation of current CG-rendered datasets, that diverse, high-quality CG assets do not scale easily. The intuition is that modern large generative models, *e.g.*, Stable Diffusion XL [24] and FLUX [25] are trained on billion-scale text-image pairs. The extensive training regime has shown its efficacy in faithfully simulating real-world distributions. The challenge of the pipeline lies in the sampling of diverse data pairs from the prior distribution inherent to generative models. As analyzed in GTA-Human [18], ensuring diversity in camera angles, poses, body shapes, and human appearances within generated human images is critical to accurately simulate real-world human distributions. This diversity is essential for improving the performance of human pose and shape (HPS) tasks by providing more representative and varied training data, especially in-the-wild data. In contrast, ensuring precise alignment between human images and generated annotations is another critical aspect. This alignment is indispensable to facilitate the effective

training of downstream tasks. DiffusionHPC [26] offers a straightforward solution by providing the model with diverse text prompts and using pretrained 3D human pose estimation (HPS) models to generate pseudo-labels. However, relying solely on text prompts lacks the granularity needed to precisely control important factors like pose, body shape, and spatial positioning. As a result, the generated 3D pseudo-labels often contain substantial noise, reducing their accuracy.

In contrast, we propose a generative method that leverages precise 3D annotations as conditions. We begin by sampling the SMPL-X parameters from large-scale human motion capture datasets such as AMASS [27]. Then, we utilize a random camera setup to render the human mesh into three spatial maps, *i.e.*, a keypoint heatmap, a depth map, and a surface normal map. These spatial maps are added as extra input conditions to the generative models, as they provide valuable information about human body’s pose, depth, and surface orientation, enhancing the model’s ability to generate more accurate outputs. Finally, we feed text prompts and these perceptual maps to a multi-condition ControlNet [28] for generating human images.

Notably, we observe existing general-purpose controllable image generators, *e.g.*, ControlNet [28], struggle to generate accurate human images even though precise spatial conditioning controls are provided. This is mainly due to the lack of high-quality training samples. To address this, we first create a large-scale human-centric dataset, each with detailed annotations including text descriptions, human poses, depth maps, and surface normals. The full data curation pipeline is outlined in Sec. 3.2. We then fine-tune a multi-condition ControlNet using this dataset to improve its performance in generating human images under spatial constraints.

Thanks to the high-quality fine-tuning data, most data samples generated by the multi-condition ControlNet demonstrate satisfactory performance. However, empirical analysis revealed instances of label noise in the initial training pairs. These issues include cases where the generated human figure and input conditions appear as mirrored pairs (see Fig. 6), or where the head orientation in the image differs from the input SMPL-X parameters (see failure cases in Supp. Mat.). To address this, we use a pre-trained segmentation model, SAM [29], to predict the human mask in the generated images. We then calculate the intersection-over-union (mIoU) between the ground-truth human mask and the predicted one, to filter out data samples with an IoU below a certain threshold. Finally, we apply a well-trained 2D dense surface estimator to refine the SMPL-X parameters using the SMPLify method [16], further improving the alignment between the

input and generated outputs.

With the aforementioned pipeline, we can finally generate a large-scale 3D human dataset in the wild, with high-quality human appearance and 3D annotations. As shown in Table 1, both mocap-based and CG-rendered datasets are limited in providing diverse human identities and in-the-wild scenes. Compared to previous datasets, our pipeline can generate diverse human identities, human interactions, and various in-the-wild scenes. Notably, the pipeline is much cheaper than both mocap-based and CG-based counterparts and is scalable to generate 3D human datasets in the wild with versatile real-world scenes.

Our contributions can be summarised as follows. **1).** We curate a large-scale, human-centric dataset with comprehensive, high-quality annotations designed for controllable human image generation. **2).** Without pursuing fancy techniques, we propose a simple yet cost-efficient pipeline to synthesize realistic and diverse human images with well-aligned annotations, including paired SMPL-X parameters and human images. Beyond human pose and shape estimation, the dataset can empower a wide range of downstream perception tasks by rendering SMPL-X mesh into corresponding annotation format, *e.g.*, human part segmentation. **3).** We verify the quality of the generated dataset on the 3D HPS task. Experimental results indicate that the proposed pipeline is compositional with CG-rendered data, enhancing performance across multiple challenging HPS benchmarks under consistent settings.

## 2 RELATED WORK

### 2.1 Human Pose and Shape Estimation Datasets

**Real-world human pose data** plays a pivotal role in achieving precision and realism in 3D HPS tasks. High-quality 3D human data is typically captured using advanced motion capture devices like Inertial Measurement Units (IMUs) [23], [27], [33] or Optical sensors [12], designed to capture precise marker movements or joint rotations. Nevertheless, the utilization of these tools may present challenges attributable to factors such as financial expenses, intricacies in configuration, and spatial constraints. To facilitate these challenges, researchers have explored alternative methods to capture pseudo labels from diverse image types, including single-view images [16], RGBD [34], and multi-view [14], eliminating the need for motion capture gear. SLOPER4D [35] consolidates data from IMU sensors, LiDAR, and RGB information to construct a large-scale urban human-scene dataset. Such methods often leverage perception models to derive 2D cues from images, which are further optimized by a 3D joint re-projecting loss.

**Synthetic human pose datasets**, developed with computer graphics techniques, have been used for many years. SUR-REAL [36] applies human skin and cloth textures to bare SMPL meshes, which lack realistic details. AGORA [32] uses high-quality static human scans for image rendering, but this routine also suffers from a high workload of scanning and rigging. However, rendering realistic, manipulable synthetic human datasets involves many challenges, including the need for diverse virtual properties for realistic data. BEDLAM [19] and Synbody [20] augment SMPL-X meshes [37] with diverse hair models and skin textures, facilitating the

simulation of physically realistic clothes and hair dynamics. These processes can be resource-intensive. Furthermore, the use of rendering engines demands many professional skills. Besides, the rendering process can be computationally expensive and time-consuming.

**Controllable human image generation** has gained great traction with the advancement of Stable Diffusion [38], [28]. Text2Human [39] uses a diffusion-based transformer sampler in response to text prompts and predicts indices from a hierarchical texture-aware codebook to conditionally generate realistic human images. HumanSD [40] introduces a skeleton-guided diffusion model with a novel heatmap loss for pose-conditioned human image generation. HyperHuman [41] proposes to jointly denoise surface normal and depth along with the synthesized RGB image conditioned with text prompt and pose skeleton.

**Generative Models for Perception Tasks** is a rapidly growing field that aims to enhance the performance of perception models by utilizing the vast prior knowledge of generative models. Several pioneering works have proposed generating perception datasets with diffusion models. For instance, [42] and [43] verified the effectiveness of datasets synthesized by generative models in fundamental perception tasks, *i.e.*, image classification, and object detection. StableRep [44] argues that training modern self-supervised methods on synthetic images from Stable Diffusion Models can yield impressive results. The learned representations often surpass those learned from real images of the same sample size. DatasetDM [45] leverages the prior of the Stable Diffusion model by training customized perception decoders upon the output of the UNet [46] and then employs it to generate pseudo labels for semantic segmentation, depth estimation, and 2D human pose estimation.

## 3 METHOD

We present **HumanWild**, a simple yet effective approach for creating versatile human body images and corresponding 3D parametric mesh annotations in a fully automated fashion, which can be used for many downstream human perception tasks, such as 2D/3D human pose and shape estimation (see Fig. 2). The core idea of the proposed pipeline is creating large-scale image-mesh-caption pairs by incorporating 2D generative models, *e.g.*, ControlNet [28] and 3D human parametric models [37]. For the sake of completeness, we give a brief review of the controllable text-to-image (T2I), image-to-image (I2I) generative models, and the 3D human parametric model, SMPL-X [37] in Sec. 3.1. Then, we show how we build large-scale human-centric datasets in Sec. 3.2 for the controllable human generation task. Next, we illustrate how we generate the initial human image-annotation pairs in Sec. 3.3. Furthermore, we show our filtering strategy for the noisy labels to get high-quality training pairs in Sec. 3.4.

### 3.1 Prerequisites

**Stable Diffusion Models** [38], [24] are text-to-image diffusion models capable of generating highly photo-realistic images given any text input. It consists of an autoencoder and a denoiser. During training, U-Net model is designed to take a textual description and noise map  $\epsilon$  as input, learning a

Data type	Datasets	Subjects	Scene	Frame	Modalities					
					RGB	D/N	K2D	K3D	B.P.	WB.P.
Real-world	Monocular	COCO [21]	-	104K	✓		✓			
		MPI-INF-3DHP [15]	8	1.4M	✓		✓	✓		
		MPII [22]	-	24K	✓		✓			
	Multi-view	HuMMan	1000	60M	✓	✓	✓	✓	✓	✓
		ZJU Mocap [30]	6	>1K	✓		✓	✓	✓	
		AIST++ [31]	30	10.1M	✓		✓	✓	✓	
	MOCAP	3DPW [23]	5	<60	✓		✓	✓	✓	
		Human3.6M [12]	11	3.6M	✓	✓	✓	✓	✓	
	Synthetic	AGORA [32]	>350	18K	✓	✓	✓	✓	✓	✓
		Synbody [20]	10K	1.2M	✓	✓	✓	✓	✓	✓
		BEDLAM [19]	217	280K	✓	✓	✓	✓	✓	✓
Generated	HumanWild	∞	∞	630K	✓	✓	✓	✓	✓	✓

TABLE 1: Comparison of different types of 3D HPS datasets.

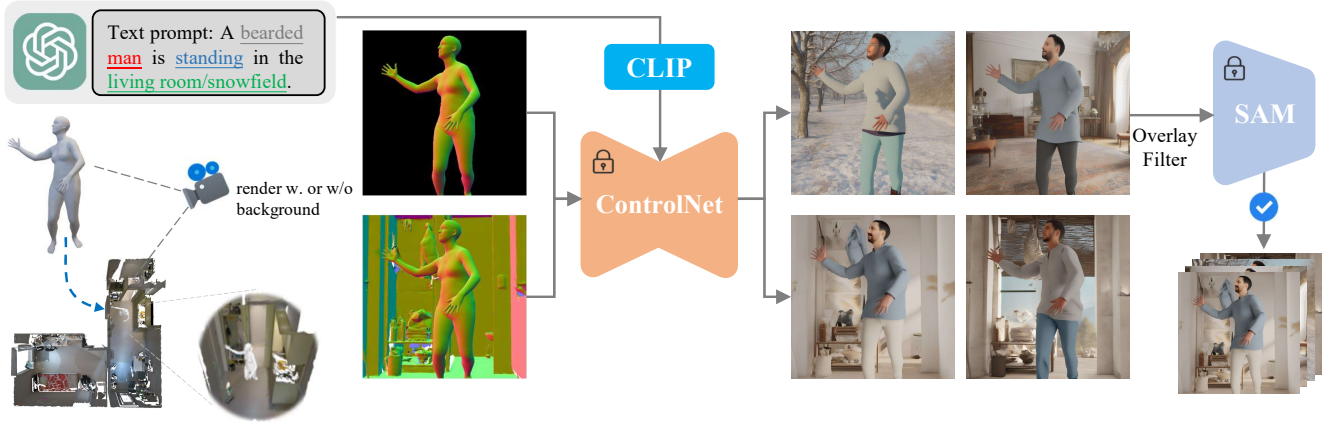


Fig. 2: The overall pipeline of the proposed controllable data generation. Our ControlNet could be conditioned on fine-grained keypoint maps, depth maps, surface normal maps, and structural text prompts. Our text prompt includes human appearance, pose, and indoor/outdoor scene types based on w. or w/o background normals.

forward noising process by gradually transforming an image latent variable, denoted as  $\bar{y} \in \mathbb{R}^{h \times w \times c}$  into a noise map  $\bar{y}_t \in \mathbb{R}^{h \times w \times c}$ :

$$y_t = \sqrt{\alpha_t} \bar{y} + \sqrt{1 - \alpha_t} \epsilon_t \quad \epsilon_t \sim \mathcal{N}(\mathbf{0}, \mathbf{I}), \quad (1)$$

where  $t = [1, \dots, T]$  is the timestep for controlling the noise level and  $\alpha_t$  is the noise scheduler [47],  $h$ ,  $w$  and  $c$  are the height, width, and channels of the latent variable. During inference, UNet takes a noise map as input and generates an approximation of the original latent variable by using a denoise scheduler [48].

**SMPL-X** [37], defined as  $M(\beta, \theta, \psi) : \mathbb{R}^{|\theta| \times |\beta| \times |\psi|} \rightarrow \mathbb{R}^{3N}$ , is a 3D wholebody human parametric model, employing shape  $\beta \in \mathbb{R}^{200}$ , expression  $\psi \in \mathbb{R}^{50}$ , and pose  $\theta \in \mathbb{R}^{55 \times 3}$  to control the entire body mesh. The function of SMPL-X provides a differentiable skinning process that uses pose, shape, and expression parameters as inputs and delivers a triangulated mesh  $V \in \mathbb{R}^{N \times 3}$  with  $N = 10475$  vertices. The reconstructed 3D joints  $J \in \mathbb{R}^{144 \times 3}$  can be obtained using a forward kinematics process. We use the SMPL-X model to represent the human body.

### 3.2 Human-centric Dataset for Human Generation

Large-scale datasets with high-quality samples, rich annotations, and diverse distributions are essential for controllable

human image generation. To address this need, we have created a comprehensive human dataset with extensive annotations. Our dataset consists of two parts: CG-rendered human images and curated human images from existing sources, such as LAION-Human [49] and other publicly available Internet datasets.

**Real-world Human.** For real-world human data collection, we filter images from LAION-2B-en [49] and COYO-700 [50] using the YOLOs human detector [51]. Next, we apply state-of-the-art perception models—DepthAnything-V2 [52], DSINE [53], and DWPose [54]—to generate corresponding depth maps, surface normal maps, and keypoint heatmaps, respectively. The curated dataset covers a broad spectrum of scenes, including diverse backgrounds and partial human regions like clothing and limbs, providing a rich variety of real-world data for further use.

**CG-rendered Human.** We also introduce a synthetic dataset to provide accurate annotations for controllable human image generation. Specifically, we utilize 630 human models from RenderPeople [55] and 660 body pose sequences from AMASS [27]. We use HDRi images with various lighting conditions as backgrounds. As shown in Fig. 3, the rendered dataset includes diverse human identities along with precise depth maps and surface normal maps without background, enhancing the dataset’s utility for various tasks.

**Fine-tune Multi-condition ControlNet.** We then use the



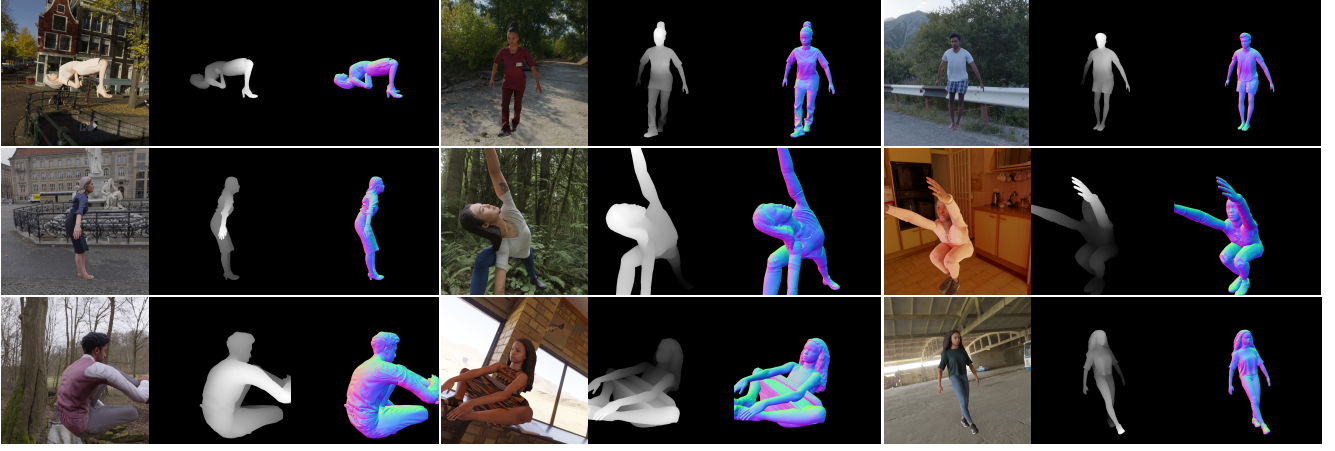


Fig. 3: Visualization of our rendered human dataset with diverse human identities and in-the-wild scenes. Each data sample contains RGB image (left), a depth map (middle), and a surface normal map (right).

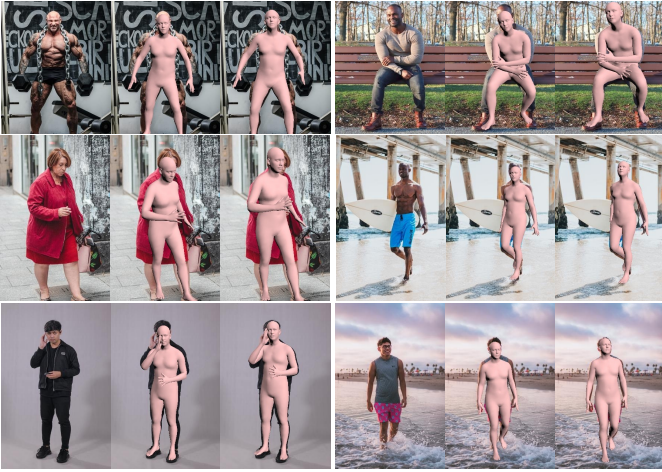


Fig. 4: Visualization of HPS estimation. For each data sample, left is the original image, middle is trained on BEDLAM dataset, right is finetuned on our HumanWild dataset.

curated dataset for fine-tuning a multi-condition ControlNet [28] based on SDXL [24] for our customized controllable human image generation. The input conditions of ControlNet are text prompts, keypoint heatmaps, depth maps, and surface normal maps. As shown in Fig. 5, our fine-tuned ControlNet are generalizable to diverse poses and shapes generated by SMPL-X, while existing ControlNet variants trained on general datasets failed in many scenes.

### 3.3 Initial Human Image and Annotation Generation

**Camera simulation.** One drawback of vision-based motion capture systems is that they need to calibrate and synchronize the camera’s intrinsic and extrinsic parameters during the capture. Thus, the collected human data are limited in terms of the scales and view diversity. On the contrary, our pipeline gets rid of the physical RGBD cameras and can simulate arbitrary human scales and body orientations. Specifically, we randomly determine the orthographic scale  $s$  of the human body, with  $s \in [0.45, 1.1]$ . We also compute the horizontal shifts  $t_x$  and  $t_y$  within the ranges  $[b_t/s, b_b/s]$  and  $[b_l/s, b_r/s]$  respectively. Here,  $b_t, b_b, b_l$ , and  $b_r$  represent

the empirical boundary values chosen based on whether a normal map is being generated for the half-body or the whole body. Following [1], [56], we determine the translation of the body as  $transl = [t_x, t_y, f/s]$ . The focal length in normalized device coordinate (NDC) space, denoted as  $f$ , can be computed using the formula  $f = 1/\tan(FoV/2)$ . Here,  $FoV$  represents the Horizontal Field of View angle, which is randomly adjusted from 25 to 120 degrees by following [19], [56]. We also augment the human body’s rotation by  $[-180^\circ, 180^\circ]$  along  $y$  axis and  $[-30^\circ, 30^\circ]$  along  $x, z$  axis.

**Image condition generation.** To synthesize realistic human images with paired pose annotations, we leverage the multi-condition ControlNet fine-tuned in Sec. 3.2, as our image generator. Existing ControlNet variants usually take a 2D keypoint heatmap, depth map, or surface normal map as condition inputs. These inputs are typically detected from real-world images by pre-trained perception models. Different from the common usage, we construct the input of ControlNet by taking advantage of the 3D human parametric model, SMPL-X. Specifically, we use existing large-scale human motion capture databases [27] with diverse body poses and shapes in SMPL-X format to render the spatial input condition maps, *i.e.*, keypoint heatmaps, depth maps, and surface normal maps. Thanks to the disentanglement of pose and shape parameters in the SMPL-X model, we can even recombine these parameters to generate a human mesh that doesn’t exist in the databases.

Upon getting the simulated camera parameters aforementioned in Sec. 3.3 and 3D human mesh from SMPL-X, we can render an existing 3D human mesh into the image plane by using perspective projection, as such, getting the corresponding source normal map, depth map, and 2D keypoint heatmap. Notably, the surface normal map is proven to be crucial to generating accurate body shapes and orientation, and the keypoint heatmap and depth map are useful for improving the alignment between the input body pose and the generated image.

**Human & scene positioning.** We offer an optional flexible background selection feature, allowing users to generate scenes based on text prompts solely or in conjunction with background-free keypoint heatmaps, depth maps, and normal maps. To integrate specific backgrounds, we randomly

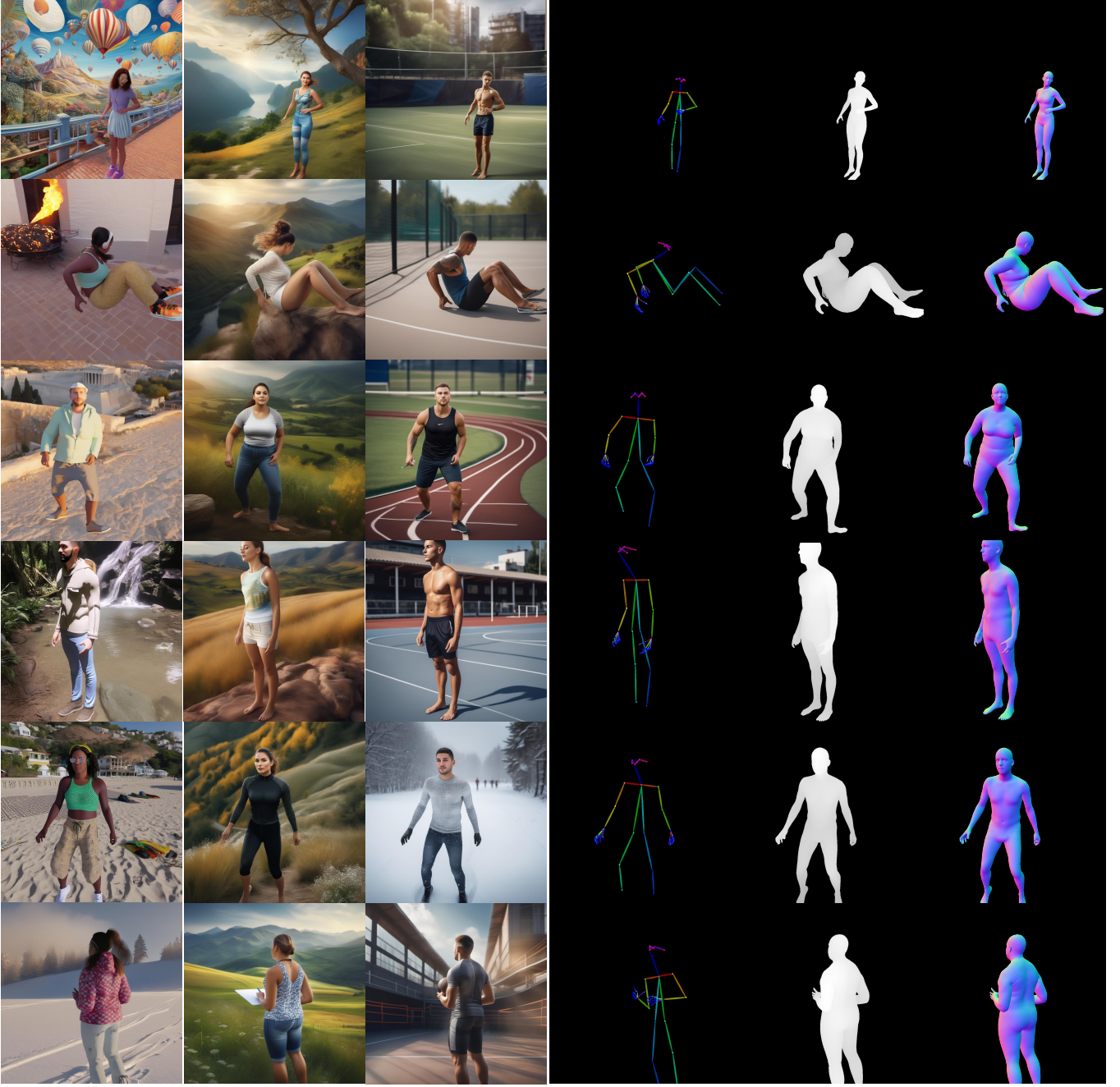


Fig. 5: Visualization of human images generated by our multi-condition generation pipeline with diverse poses and scenes. For each data sample, the first column is generated from the ControlNet before revision. **The second and third columns are generated from our revised model.** The fourth, fifth, and sixth columns are keypoint heatmap, depth map, and surface normal map rendered from the SMPL-X model.

select scene meshes from the ScanNet++ dataset [57]. We first utilize Octree [58] to partition the room mesh into discrete voxels. With vertex-level classification annotations, we efficiently identify ground plane normals and height to anchor the human mesh. We randomly allocate human mesh within unoccupied areas of the voxel space. Subsequently, we refine human mesh positioning by optimizing the translation using the Chamfer distance to preclude inter-mesh collisions. Finally, we simulate a random camera perspective. The intrinsic matrix is obtained with the previous rules, while the

extrinsic matrix is crafted using a random azimuth angle. We sample the camera’s height range  $[-1\text{m}, +1\text{m}]$  relative to the pelvis height, and look at a random point on the human torso, to achieve a realistic viewpoint. The visualization results can be seen in the appendix.

**Text prompt generation.** To create controllable and diverse in-the-wild background scenes, we can use text prompts to provide background information. Moreover, the human body’s spatial maps are not fine-grained enough to determine the gender and appearance of a human. Thus, we incorporate



a structured text prompt template to handle this issue. In particular, we designed a simple text template as “A {gender} {action} {environment}”. The gender of the person is determined by the SMPL-X annotations. The environment is generated by a large language model, *i.e.*, ChatGPT [59] and LLAMA [60]. To create photo-realistic humans, we also feed negative text prompts, *e.g.*, “ugly, extra limbs, poorly drawn face, poorly drawn hands, poorly drawn feet”, to the model.

Finally, we have all of the input conditions of the multi-condition ControlNet. We apply a total of 40 inference steps for each sample. The generated images are up to  $1024 \times 1024$  resolution. The generated images and the input conditions (SMPL-X parameters) are regarded as the initial data pairs.

### 3.4 Label Denoising

The generated images are not always well-aligned with the input conditions. For example, an incorrect case is that the generated human and the input conditions form a mirror pair, as shown in Fig. 6. To resolve this problem, we employ an off-the-shelf foundation segmentation model, *i.e.*, SAM [29], to filter negative samples from the final dataset. Specifically, we first calculate the ground-truth mesh segmentation mask by rendering the 3D mesh into the image plane. Then, we sample a random point coordinate from the ground-truth segmentation mask and feed the generated image and this point coordinate into the SAM model, thereby we can get the predicted human mask for the generated image. Finally, we compute the intersection-over-union (IoU) metric between the ground-truth mask and the prediction mask. We filter data samples with IoU lower than 0.8.

To further improve the alignment between the generated human images and SMPL-X pose parameters, we train a sparse 2D surface estimator by using RTMPose [61] architecture to estimate a total of 128 sparse 2D vertices sampled from dense SMPL-X vertices [62]. The input resolution of the detector is  $512 \times 384$ . As our generated images have accurate camera intrinsics, we can project the ground-truth 3D SMPL-X vertices into 2D vertices using perspective projection. Then, we can optimize the original SMPL-X pose parameters with SMPLify [16]. Note that we only optimize the body pose parameters for 20 iterations and make the shape parameters fixed.

## 4 EXPERIMENTS

### 4.1 Human-centered Datasets for training ControlNet

In this section, we list our datasets for fine-tuning the multi-condition ControlNet in terms of the number of subjects, the number of scenes, and the details of diversity. Overall, we use three datasets for fine-tuning an existing variant. The RenderedHuman dataset contains 202,667 human images, distinguishing itself by providing an unparalleled wealth of precise annotations, including texts, keypoints, depth, and surface maps. The PexHuman is collected with more than 120 daily human activities, including 100,880 images. We also filter the Laion5B dataset by a human detector, YOLOs [51], where only images with fewer than 3 humans are kept. We generate keypoints, depth, and surface maps for PexHuman and LaionHuman with DWPose [54], DepthAnythingV2 [63], and DSINE [53], separately. To get

Dataset	Data Type	# Samples	# Scenes	# Identities
LaionHuman	real	233,728	> 200K	> 200K
PexelHuman	real	100,880	> 100K	> 100K
RenderHuman	Synthetic	202,667	660	630

TABLE 2: An overview of all datasets for fine-tuning multi-condition ControlNet.

the text description of the human images, we leverage a multi-modality vision-language model, CogVLM [64], to generate detailed image captions.

### 4.2 Implement Details and Evaluation Metrics

To illustrate the effectiveness and efficiency of our proposed **HumanWild**, we report the Frechet Inception Distance (FID [65]) and the Kernel Inception Distance (KID [66]), which are widely used to measure the quality of the synthesized images. We measure the alignment accuracy between the SMPLX-rendered mask and the generated images with mean intersection over union (mIoU). We use standard metrics to evaluate body pose and shape accuracy. PVE and MPJPE represent the average error in vertices and joints positions, respectively, after aligning the pelvis. PA-MPJPE further aligns the rotation and scale before computing distance. PVE-T-SC is a per-vertex error in a neutral pose (T-pose) after scale correction. For a fair comparison with the counterpart pure CG pipeline, we sample SMPL-X pose and shape parameters from the AMASS [27] dataset and render them into surface normal maps with random camera parameters illustrated in Sec. 3. We re-implemented a regression-based HPS method, CLIFF [4], for evaluating the effectiveness of the synthesized dataset on a variety of evaluation benchmarks, 3DPW [23], AGORA [32], EgoBody [67], RICH [68], and SSP-3D [69] (for shape evaluation).

Unless specified, all HPS models are trained on the CLIFF [4] model with an HRNet-48 [70] backbone. Following BEDLAM [19], the supervision losses are a combination of MSE loss on model parameters, projected keypoints, 3D joints, and an L1 loss on 3D vertices.

### 4.3 Ablation on ControlNet Input Conditions

In the initial stages of our research, we employed various input conditions, including 2D keypoint heatmaps, depth images, and normal images, to generate data samples. However, a notable challenge emerged with regard to the ambiguity inherent in both the keypoint and depth conditions. Specifically, the diffusion model struggled to accurately discern the front and back of individuals depicted in these data modalities and had difficulty in aligning generated hands and faces with ground-truths (See Sup. Mat. for some failure cases), yet we found that surface normal conditioning can greatly reduce this kind of ambiguity. Thus, we choose a multi-condition variant of the ControlNet, which can optionally treat keypoint, depth, and surface normal maps as input. Table 3 compares our trained ControlNet with two publicly available keypoint-based and depth-based ControlNets [63], [71] in terms of generated image quality and image/ground-truth alignment accuracy. In order to ensure equitable comparison, all ControlNets employ aligned sets of 1,000 input conditions derived from identical SMPL-X parameters

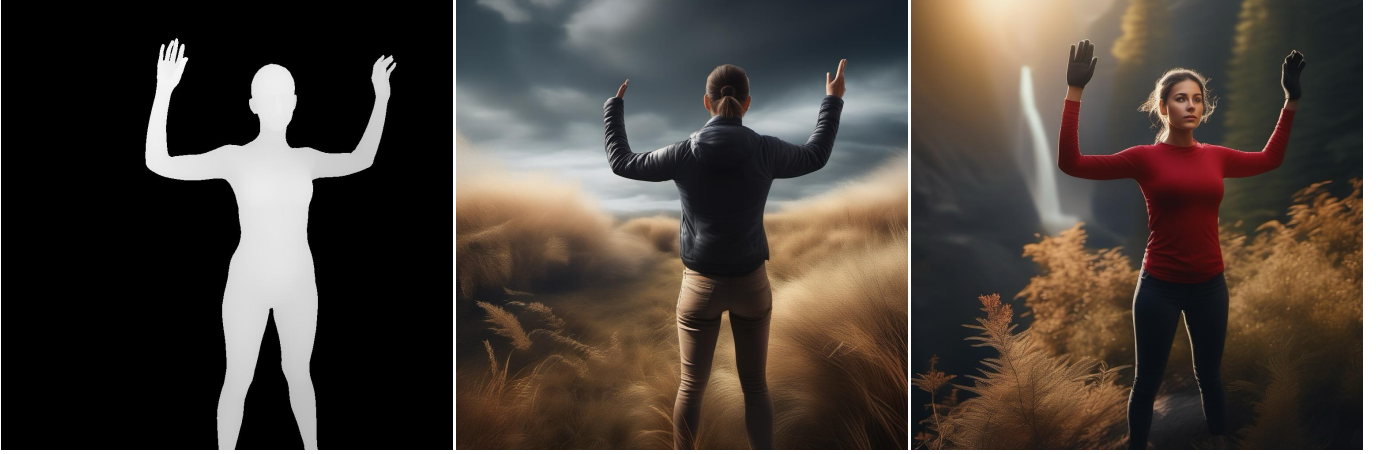


Fig. 6: Analysis of Mirror Image Generation from Depth Maps: This visualization demonstrates the correction of a common failure mode. The leftmost image is the guiding depth map. The middle image is an incorrect output where the model mistakenly generates the person’s back. The rightmost image shows the desired outcome, a correctly rendered frontal view.

and camera specifications. The results demonstrate that our ControlNet consistently outperforms the keypoint-based and depth-based ControlNet.

ControlNet Condition	Image Quality		Alignment Accuracy
	FID ↓	KID ↓	mIoU ↑
Keypoint [71]	29.6	2.92	41.3
Depth [63]	28.1	2.87	49.2
Normal	24.5	2.83	56.8
All conditions	<b>22.5</b>	<b>2.74</b>	<b>59.2</b>

TABLE 3: Ablation of different input conditions of ControlNet.

We also visualize the generated images by a general depth-conditioned ControlNet, and our finetuned multi-condition ControlNet in Fig. 7. As we can see, the general depth-conditioned ControlNet trained on general datasets fails to generate accurate fingers, poses, and limited background scenes, while our fine-tuned multi-condition ControlNet can generate diverse photo-realistic humans tightly aligned with the input condition.

#### 4.4 Verification of the Necessity of In-the-wild 3D Data

Previous studies, HMR-Benchmark [72] and BEDLAM [19] point out that different backbone initialization strategies profoundly impact an HPS model’s convergence speed and final accuracy. HMR-benchmarks [72] conduct a systematic analysis by initializing the same backbone pre-trained with different sources, *i.e.*, ImageNet classification weights, 2D pose estimation weights from MPII, and COCO. As shown in the first three columns of Table 6 show the results are trained on real datasets. The conclusion is that COCO keypoint pretraining helps HPS models trained on real datasets achieve the best performance.

To verify whether the conclusion still holds for CG-rendered synthetic datasets, columns 4 to 6 of the Table 6 elucidate the impact of backbone pretraining on BEDLAM [19] and AGORA [32]. A consistent conclusion is drawn that COCO keypoint pretraining also has a great positive impact on CG-rendered datasets.

Based on the above observation, we posit that neither indoor-mocap datasets nor CG-rendered datasets offer a sufficiently varied array of photo-realistic, in-the-wild scenes. Consequently, the HPS network, which is not initialized with large-scale in-the-wild data pretraining, struggles to perform well on unseen scenes and has limited generalization capability. As our generated data contains diverse in-the-wild scenes, we add the data generated by our pipeline for training HPS models. As we can see in the final column of Table 6, the inclusion of in-the-wild synthesized data generated by **HumanWild** can further enhance the HPS performance of the CG-rendered datasets. Hence, data synthesized by diffusion models can effectively complement CG-rendered data by featuring diverse human identities and real-world scenes.

Training Data	PA-MPJPE↓	MPJPE↓	PVE↓
PDHuman	102.4	159.1	168.0
<b>HumanWild</b>	<b>90.0</b>	<b>151.8</b>	<b>160.9</b>

TABLE 4: HPS results on SPEC-MTP.

Training Data	MPJPE ↓	PA-MPJPE ↓	PVE ↓	PA-PVE ↓
B+A+P	143.1	94.9	163.9	95.7
<b>B+A+P+H</b>	<b>134.6</b>	<b>89.1</b>	<b>154.1</b>	<b>88.9</b>

TABLE 5: HPS results on MOYO.

#### 4.5 Data Scale-up Ablation Study

We perform experiments to show the effectiveness of the generated datasets by studying the scaling law of the amount of data and the model sizes in Table 7. Notably, our training set is independent of the evaluation benchmarks in Table 7. We show results with various ViT backbones and percentages of the proposed dataset. It is observed that 1). Scale-up synthetic training data generated by **HumanWild** leads to better performance. 2). A larger backbone benefits more from a larger synthetic training dataset.



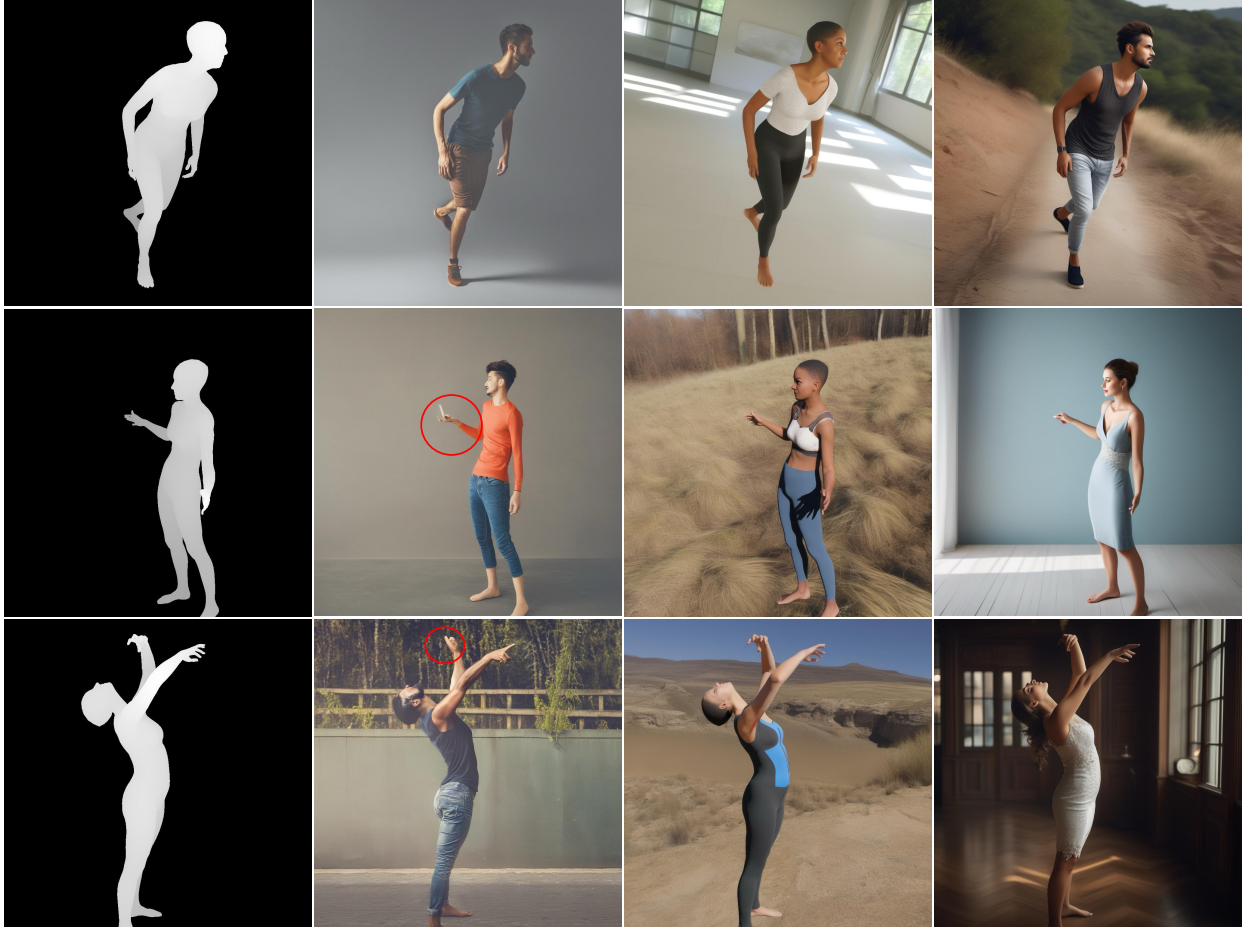


Fig. 7: Visualization of a general depth-conditioned ControlNet, and our finetuned multi-condition ControlNet. The first column is the input depth condition. The second column is the prediction from the general depth-conditioned ControlNet. The third column is our v1 model. The fourth column is our current v2 model.

Method	Dataset	Pretrain	PA-MPJPE↓	MPJPE↓	PVE↓	PVE-T-SC↓
PARE [73], [72]	R	ImageNet	54.8	N/A	N/A	N/A
PARE [73], [72]	R	MPII	51.5	N/A	N/A	N/A
PARE [73], [72]	R	COCO	49.5	N/A	N/A	N/A
CLIFF [4], [19]	B+A	scratch	61.7	96.5	115.0	N/A
CLIFF [4], [19]	B+A	ImageNet	51.8	82.1	96.9	N/A
CLIFF [4], [19]	B+A	COCO	47.4	73.0	86.6	14.2
CLIFF [4], [19]	B+A+H	COCO	<b>44.9</b>	<b>70.2</b>	<b>82.7</b>	<b>13.9</b>

TABLE 6: Ablation experiments on 3D pose and shape estimation. ‘R’ denotes mixed real-world datasets, ‘H’ denotes **HumanWild**, ‘B’ denotes BEDLAM and ‘A’ denotes AGORA. PA-MPJPE, MPJPE and PVE are evaluated on 3DPW. PVE-T-SC is evaluated on SSP-3D.

#### 4.6 Comparing with Other Real/Synthetic Datasets

In Table 8, we analyze the performance of different training datasets using mixed strategies on CLIFF with HRNet-W48 backbone. Key findings are: 1). Pure CG-rendered dataset outperforms real-world data (motion-capture, pseudo-labeled) on 3DPW and RICH datasets, suggesting the effectiveness of the synthetic data. 2). Solely training on HumanWild yields slightly lower performance than BEDLAM; we conjecture that there still exists some levels of label noise, especially in hand and face poses. 3). Combining HumanWild with CG-rendered datasets (BEDLAM, AGORA) and marker-based dataset (3DPW) enhances performance, which demonstrates

the flexibility of **HumanWild**, *i.e.*, can be integrated with existing datasets to boost the estimation performance.

These results provide additional validation for the efficacy of the generated HumanWild dataset. Specifically, they demonstrate that incorporating HumanWild data enables the HPS regressor to encounter a more diverse range of scenarios, thereby enhancing its ability to generalize to in-the-wild scenes.

#### 4.7 Result on Challenging Benchmarks

To verify the effectiveness of **HumanWild** on different scenerios, we report the detailed performance on three

#Crops	#Inst.	Model	#Param.	AGORA [32]	EgoBody [67]	RICH [74]	3DPW [23]	H36M [12]	MPE
25%	0.19M	ViT-S	23M	125.0	114.2	116.5	118.2	102.3	115.2
50%	0.39M	ViT-S	23M	116.2	103.6	104.1	110.4	95.6	106.0
100%	0.63M	ViT-S	23M	106.8	97.3	107.7	106.5	87.1	101.1
100%	0.63M	ViT-B	88M	103.6	94.2	105.1	103.5	82.5	97.8
100%	0.63M	ViT-L	305M	97.5	85.6	97.2	97.4	75.7	90.7
100%	0.63M	ViT-H	633M	90.2	82.3	92.1	90.3	72.4	85.5

TABLE 7: **Scale-up ablation.** We study the scaling law of the amount of data and the model sizes. The metrics are MPJPE for Human36M [12] and PVE for other evaluation benchmarks. Foundation models are named “ViT-M”, where M indicates the size of ViT backbone (S, B, L, H). MPE: mean primary error cross 5 evaluation benchmarks. AGORA uses the validation set, and EgoBody uses the EgoSet.

Methods	Training Data	3DPW (14)			RICH (24)		
		PA-MPJPE↓	MPJPE↓	PVE↓	PA-MPJPE↓	MPJPE↓	PVE↓
HMR [1]	Real	76.7	130	N/A	90.0	158.3	186.0
SPIN [75]	Real	59.2	96.9	116.4	69.7	122.9	144.2
SPEC [76]	Real	53.2	96.5	118.5	72.5	127.5	146.5
PARE [73]	Real	50.9	82.0	97.9	64.9	104.0	119.7
HybrIK [3]	Real	48.8	80	94.5	56.4	96.8	110.4
CLIFF [4], [19]	Real	46.4	73.9	87.6	55.7	90.0	102.0
CLIFF [4], [19]	B	50.5	76.1	90.6	-	-	-
CLIFF [4], [19]	H	51.4	83.9	96.4	-	-	-
CLIFF [4], [19]	B+A	46.6	72.0	85.0	51.2	84.5	96.6
CLIFF [4], [19]	H+A	47.5	74.1	87.8	51.9	85.3	97.4
CLIFF[4], [19]	H+B+A	<b>44.9</b>	<b>70.4</b>	<b>82.0</b>	<b>51.0</b>	<b>84.4</b>	<b>96.1</b>
CLIFF[4], [19]	B+A+P	43.0	66.9	78.5	50.2	84.4	95.6
CLIFF[4], [19]	H+B+A+P	<b>41.3</b>	<b>65.2</b>	<b>76.7</b>	<b>48.4</b>	<b>79.7</b>	<b>91.1</b>
CLIFF[4], [19]	H+B+A+P+R	45.5	71.3	84.3	52.6	86.4	98.3

TABLE 8: Reconstruction error on 3DPW and RICH. ‘R’ denotes mixed real-world datasets, ‘H’ denotes **HumanWild**, ‘B’ denotes BEDLAM [19], and ‘A’ denotes AGORA [32]. ‘P’ denotes 3DPW [23].

challenging benchmarks. Firstly, we evaluate the capability of **HumanWild** in handling perspective distortion human pose and shape estimation, by performing fair ablation using Zolly [56] with ResNet50 [77] backbone. The results in Table 4 show that **HumanWild** dataset achieves higher generalization performance on SPEC-MTP [76] when compared with PDhuman [56], which is a CG-rendered perspective distortion dataset. Secondly, MOYO [13] encompasses challenging yoga poses not present in BEDLAM and **HumanWild** datasets, providing a unique testbed for evaluating the model’s generalization ability on hard poses. The results in Table 5 demonstrate that **HumanWild**, complements existing datasets, resulting in improved generalization performance on the MOYO test set.

We show AGORA test set results in Table 9, our analysis reveals that while Humanwild demonstrates superior performance over BEDLAM on body metrics, it exhibits relatively poorer performance on hand and face metrics, particularly evident in comparison to the AGORA test set. We hypothesize that the alignment of hand and facial annotations with generated images remains noisy, primarily due to inherent limitations in current diffusion models’ ability to accurately generate hand poses, particularly within small resolutions.

#### 4.8 Visualization on in-the-wild scenes

In this section, we show visualization results of two types of CLIFF estimators with the same HRNet-W48 backbone [70]. One CLIFF is trained on the BEDLAM dataset (we use the official weights released by authors), another is trained on both BEDLAM and HumanWild datasets. As we can see from Fig. 4, our finetuned CLIFF estimator has more accurate pose and shape estimation results in diverse scenes, demonstrating the effectiveness of our data to help existing models have better generalization performance.

## 5 LIMITATIONS AND FUTURE WORK

**Limitations in photo-realism.** We observe that our finetuned ControlNet model can generate images that are either blurry or lack photorealism. This issue stems from that the underlying SDXL base model possesses limited capacity for photorealistic generation. As shown in Fig. 8, the SDXL base model tends to generate images with a blurred background. Given recent advancements, such as the FLUX [25] model, which demonstrate more promising results in synthesizing high-resolution and realistic human imagery, future efforts should be directed toward scaling up controllable generative models to achieve greater photorealism.

Method	NMVE↓ (mm)		NMJE↓ (mm)		MVE↓ (mm)					MPJPE↓ (mm)				
	All	Body	All	Body	All	Body	Face	LHand	RHand	All	Body	Face	LHand	RHand
BEDLAM [19]	179.5	132.2	177.5	131.4	131.0	96.5	25.8	38.8	39.0	129.6	95.9	27.8	36.6	36.7
Hand4Whole [78]†	144.1	96.0	141.1	92.7	135.5	90.2	41.6	46.3	48.1	132.6	87.1	46.1	44.3	46.2
BEDLAM [19]†	142.2	102.1	141.0	101.8	<b>103.8</b>	74.5	<b>23.1</b>	<b>31.7</b>	<b>33.2</b>	<b>102.9</b>	74.3	<b>24.7</b>	<b>29.9</b>	<b>31.3</b>
PyMaF-X [79]†	141.2	94.4	140.0	93.5	125.7	84.0	35.0	44.6	45.6	124.6	83.2	37.9	42.5	43.7
OSX [74]*	130.6	85.3	127.6	83.3	122.8	80.2	36.2	45.4	46.1	119.9	78.3	37.9	43.0	43.9
<b>HumanWild †</b>	<b>120.5</b>	<b>73.7</b>	<b>115.7</b>	<b>72.3</b>	112.1	<b>68.5</b>	37.0	46.7	47.0	107.6	<b>67.2</b>	38.5	41.2	41.4

TABLE 9: **AGORA test set.** † denotes the methods that are finetuned on the AGORA training set. \* denotes the methods that are trained on AGORA training set only.



Fig. 8: Images generated directly from SDXL [24]. Text prompt: a beautiful woman wearing a loose dress on the beach.

**Limitations in multi-Human synthesis.** The current pipeline effectively generates high-quality images containing one to three human subjects. When the number of individuals increases, their scale within the image decreases, leading to poor alignment with the inputs of the guiding depth, keypointmap. Consequently, the resulting data is unsuitable for training human pose and shape models. Future research could leverage recent generative image editing models, such as Bagel [80] and Flux Kontext [81], to translate our computer-rendered datasets into more photorealistic domains.

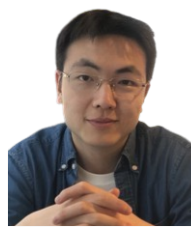
## 6 DISCUSSION AND CONCLUSIONS

Based on the experiments, we can answer the question “Is synthetic data generated by generative models complementary to CG-rendered data for the 3D HPS task?” Our results strongly suggest that through the integration of 3D human priors with pretrained diffusion models, it becomes feasible to produce high-fidelity pseudo labels encompassing a wide array of real-world scenarios. As the landscape sees the emergence of increasingly large generative models, there arises a promising prospect for the expansion of diverse 3D human training datasets without intricate mocap systems and CG pipelines. We hope that our endeavors could pave the way for leveraging generative models to generate high-quality datasets, which are conducive to enhancing the efficacy of 3D human perception tasks.

Our pipeline holds significant potential for various related tasks where acquiring high-quality data pairs is difficult, such as 3D animal pose estimation and 3D reconstruction of human-object or human-human interactions. Addressing these challenges will require further advancements in our methodology, which we will explore in future research.



**Yongtao Ge** Yongtao Ge is currently a PhD student at the University of Adelaide. He has published papers on top-tier conferences, including SIGGRAPH, ICCV, ECCV, ICLR and AAAI. His research interests mainly lies in the intersection of computer vision and computer graphics, including human-centered digitization and world models.



**Hao Chen** is an Assistant Professor of Computer Science at Zhejiang University. Prior to that, he worked as a researcher at Noah's Ark Lab at Huawei. He got his PhD degree from University of Adelaide. He obtained his undergraduate and master degrees from Zhejiang University.



**Wenjia Wang** is currently pursuing his PhD degree in The University of Hongkong, advised by Prof. Taku Komura and Prof. Wenping Wang. Prior to that, he worked in computer vision in SenseTime and Tencent, from 2019 to 2022. He has published papers on top-tier conferences, including CVPR, ECCV, ICCV, and IJCAI.

**Chunhua Shen** is a Chair Professor of Computer Science at Zhejiang University and Zhejiang University of Technology. He was with Amazon Australia, and The University of Adelaide, Australia. His research interest is Computer Vision and Machine Learning.



**Yongfan Chen** was a master student at Zhejiang University, under the supervision of Prof. Chunhua Shen. Prior to this, he earned his bachelor's degree in Computer Science and Technology from Huazhong University of Science and Technology. His current research primarily focuses on computer vision, pose estimation and generative models.



**Fanzhou Wang** is currently an Algorithm Researcher at SenseTime Group Inc. Prior to that, she received her M.S. degree and B.E. degree from Southeast University in 2023 and 2020. Her research interests include synthetic data and computer graphics.



**Lei Yang** is currently a Research Director at SenseTime Group Inc., under the supervision of Prof. Xiaogang Wang. Prior to that, Lei received his PhD degree from the Chinese University of Hong Kong in 2020, advised by Prof. Dahua Lin and Prof. Xiaoou Tang. Before that, Lei obtained his B.E. degree from Tsinghua University in 2015. He has published over 10 papers on top conferences in relevant fields, including CVPR, ICCV, ECCV, AAAI, SIGGRAPH and RSS.



## REFERENCES

- [1] Angjoo Kanazawa, Michael J Black, David W Jacobs, and Jitendra Malik. End-to-end recovery of human shape and pose. In *Proc. IEEE Conf. Comp. Vis. Patt. Recogn.*, pages 7122–7131, 2018.
- [2] Kevin Lin, Lijuan Wang, and Zicheng Liu. Mesh graphormer. In *Proc. IEEE Int. Conf. Comp. Vis.*, pages 12939–12948, 2021.
- [3] Jiefeng Li, Chao Xu, Zhicun Chen, Siyuan Bian, Lixin Yang, and Cewu Lu. Hybrik: A hybrid analytical-neural inverse kinematics solution for 3d human pose and shape estimation. In *Proc. IEEE Conf. Comp. Vis. Patt. Recogn.*, pages 3383–3393, 2021.
- [4] Zhihao Li, Jianzhuang Liu, Zhensong Zhang, Songcen Xu, and Youliang Yan. Cliff: Carrying location information in full frames into human pose and shape estimation. *arXiv: Comp. Res. Repository*, 2022.
- [5] Zhiyang Dou, Qingxuan Wu, Cheng Lin, Zeyu Cao, Qiangqiang Wu, Weilin Wan, Taku Komura, and Wenping Wang. Tore: Token reduction for efficient human mesh recovery with transformer. *arXiv preprint arXiv:2211.10705*, 2022.
- [6] Zhiyang Dou, Xuelin Chen, Qingnan Fan, Taku Komura, and Wenping Wang. C-ase: Learning conditional adversarial skill embeddings for physics-based characters. In *SIGGRAPH Asia 2023 Conference Papers*, pages 1–11, 2023.
- [7] Zeqi Xiao, Tai Wang, Jingbo Wang, Jinkun Cao, Wenwei Zhang, Bo Dai, Dahua Lin, and Jiangmiao Pang. Unified human-scene interaction via prompted chain-of-contacts. *arXiv preprint arXiv:2309.07918*, 2023.
- [8] Jingbo Wang, Ye Yuan, Zhengyi Luo, Kevin Xie, Dahua Lin, Umar Iqbal, Sanja Fidler, and Sameh Khamis. Learning human dynamics in autonomous driving scenarios. In *Proceedings of the IEEE/CVF International Conference on Computer Vision*, pages 20796–20806, 2023.
- [9] Wenyang Zhou, Zhiyang Dou, Zeyu Cao, Zhouyingcheng Liao, Jingbo Wang, Wenjia Wang, Yuan Liu, Taku Komura, Wenping Wang, and Lingjie Liu. Emdm: Efficient motion diffusion model for fast, high-quality motion generation. *arXiv preprint arXiv:2312.02256*, 2023.
- [10] Weilin Wan, Zhiyang Dou, Taku Komura, Wenping Wang, Dinesh Jayaraman, and Lingjie Liu. Tlcontrol: Trajectory and language control for human motion synthesis. *arXiv preprint arXiv:2311.17135*, 2023.
- [11] Jionghao Wang, Yuan Liu, Zhiyang Dou, Zhengming Yu, Yongqing Liang, Xin Li, Wenping Wang, Rong Xie, and Li Song. Disentangled clothed avatargeneration from text descriptions. *arXiv preprint arXiv:2312.05295*, 2023.
- [12] Catalin Ionescu, Dragos Papava, Vlad Olaru, and Cristian Sminchisescu. Human3.6m: Large scale datasets and predictive methods for 3d human sensing in natural environments. *IEEE Trans. Pattern Anal. Mach. Intell.*, 36(7):1325–1339, 2013.
- [13] Shashank Tripathi, Lea Müller, Chun-Hao P. Huang, Taheri Omid, Michael J. Black, and Dimitrios Tzionas. 3D human pose estimation via intuitive physics. In *Proc. IEEE Conf. Comp. Vis. Patt. Recogn.*, June 2023.
- [14] Zhongang Cai, Daxuan Ren, Ailing Zeng, Zhengyu Lin, Tao Yu, Wenjia Wang, Xiangyu Fan, Yang Gao, Yifan Yu, Liang Pan, et al. Humman: Multi-modal 4d human dataset for versatile sensing and modeling. In *Proc. Eur. Conf. Comp. Vis.*, pages 557–577. Springer, 2022.
- [15] Dushyant Mehta, Helge Rhodin, Dan Casas, Pascal Fua, Oleksandr Sotnychenko, Weipeng Xu, and Christian Theobalt. Monocular 3D human pose estimation in the wild using improved CNN supervision. In *Int. Conf. 3D. Vis.*, 2017.
- [16] Federica Bogo, Angjoo Kanazawa, Christoph Lassner, Peter Gehler, Javier Romero, and Michael J Black. Keep it smpl: Automatic estimation of 3d human pose and shape from a single image. In *Proc. Eur. Conf. Comp. Vis.*, pages 561–578. Springer, 2016.
- [17] Hanbyul Joo, Natalia Neverova, and Andrea Vedaldi. Exemplar fine-tuning for 3d human model fitting towards in-the-wild 3d human pose estimation. In *Int. Conf. 3D. Vis.*, pages 42–52. IEEE, 2021.
- [18] Zhongang Cai, Mingyuan Zhang, Jiawei Ren, Chen Wei, Daxuan Ren, Zhengyu Lin, Haiyu Zhao, Lei Yang, Chen Change Loy, and Ziwei Liu. Playing for 3d human recovery. *IEEE Transactions on Pattern Analysis and Machine Intelligence*, pages 1–12, 2024.
- [19] Michael J Black, Priyanka Patel, Joachim Tesch, and Jinlong Yang. Bedlam: A synthetic dataset of bodies exhibiting detailed lifelike animated motion. In *Proc. IEEE Conf. Comp. Vis. Patt. Recogn.*, pages 8726–8737, 2023.
- [20] Zhitao Yang, Zhongang Cai, Haiyi Mei, Shuai Liu, Zhaoxi Chen, Weiye Xiao, Yukun Wei, Zhongfei Qing, Chen Wei, Bo Dai, et al. Synbody: Synthetic dataset with layered human models for 3d human perception and modeling. *arXiv preprint arXiv:2303.17368*, 2023.
- [21] Tsung-Yi Lin, Michael Maire, Serge Belongie, James Hays, Pietro Perona, Deva Ramanan, Piotr Dollár, and C Lawrence Zitnick. Microsoft coco: Common objects in context. In *Proc. Eur. Conf. Comp. Vis.*, 2014.
- [22] Mykhaylo Andriluka, Leonid Pishchulin, Peter Gehler, and Bernt Schiele. 2d human pose estimation: New benchmark and state of the art analysis. In *Proc. IEEE Conf. Comp. Vis. Patt. Recogn.*, pages 3686–3693, 2014.
- [23] Timo von Marcard, Roberto Henschel, Michael Black, Bodo Rosenhahn, and Gerard Pons-Moll. Recovering accurate 3D human pose in the wild using IMUs and a moving camera. In *Proc. Eur. Conf. Comp. Vis.*, 2018.
- [24] Dustin Podell, Zion English, Kyle Lacey, Andreas Blattmann, Tim Dockhorn, Jonas Müller, Joe Penna, and Robin Rombach. Sdxl: improving latent diffusion models for high-resolution image synthesis. *arXiv preprint arXiv:2307.01952*, 2023.
- [25] Black Forest Labs. Flux. <https://github.com/black-forest-labs/flux>, 2024.
- [26] Zhenzhen Weng, Laura Bravo-Sánchez, and Serena Yeung. Diffusion-hpc: Generating synthetic images with realistic humans. *arXiv preprint arXiv:2303.09541*, 2023.
- [27] Naureen Mahmood, Nima Ghorbani, Nikolaus F Troje, Gerard Pons-Moll, and Michael J Black. Amass: Archive of motion capture as surface shapes. In *Proc. IEEE Int. Conf. Comp. Vis.*, pages 5442–5451, 2019.
- [28] Lvmin Zhang and Maneesh Agrawala. Adding conditional control to text-to-image diffusion models. *arXiv preprint arXiv:2302.05543*, 2023.
- [29] Alexander Kirillov, Eric Mintun, Nikhila Ravi, Hanzi Mao, Chloe Rolland, Laura Gustafson, Tete Xiao, Spencer Whitehead, Alexander C. Berg, Wan-Yen Lo, Piotr Dollár, and Ross Girshick. Segment anything. *arXiv:2304.02643*, 2023.
- [30] Sida Peng, Yuanqing Zhang, Yinghao Xu, Qianqian Wang, Qing Shuai, Hujun Bao, and Xiaowei Zhou. Neural body: Implicit neural representations with structured latent codes for novel view synthesis of dynamic humans. In *Proc. IEEE Conf. Comp. Vis. Patt. Recogn.*, pages 9054–9063, 2021.
- [31] Ruilong Li, Shan Yang, David A Ross, and Angjoo Kanazawa. Ai choreographer: Music conditioned 3d dance generation with aist++. In *Proceedings of the IEEE/CVF International Conference on Computer Vision*, pages 13401–13412, 2021.
- [32] Priyanka Patel, Chun-Hao P. Huang, Joachim Tesch, David T. Hoffmann, Shashank Tripathi, and Michael J. Black. AGORA: Avatars in geography optimized for regression analysis. In *Proc. IEEE Conf. Comp. Vis. Patt. Recogn.*, June 2021.
- [33] Leonid Sigal, Alexandru O Balan, and Michael J Black. Humaneva: Synchronized video and motion capture dataset and baseline algorithm for evaluation of articulated human motion. *International journal of computer vision*, 87(1-2):4–27, 2010.
- [34] Mohamed Hassan, Vasileios Choutas, Dimitrios Tzionas, and Michael J Black. Resolving 3d human pose ambiguities with 3d scene constraints. In *Proc. IEEE Int. Conf. Comp. Vis.*, pages 2282–2292, 2019.
- [35] Yudi Dai, YiTai Lin, XiPing Lin, Chenglu Wen, Lan Xu, Hongwei Yi, Siqi Shen, Yuexin Ma, and Cheng Wang. Sloper4d: A scene-aware dataset for global 4d human pose estimation in urban environments. In *Proc. IEEE Conf. Comp. Vis. Patt. Recogn.*, pages 682–692, 2023.
- [36] Gül Varol, Javier Romero, Xavier Martin, Naureen Mahmood, Michael J. Black, Ivan Laptev, and Cordelia Schmid. Learning from synthetic humans. In *Proc. IEEE Conf. Comp. Vis. Patt. Recogn.*, 2017.
- [37] Georgios Pavlakos, Vasileios Choutas, Nima Ghorbani, Timo Bolkart, Ahmed AA Osman, Dimitrios Tzionas, and Michael J Black. Expressive body capture: 3d hands, face, and body from a single image. In *Proc. IEEE Conf. Comp. Vis. Patt. Recogn.*, pages 10975–10985, 2019.
- [38] Robin Rombach, Andreas Blattmann, Dominik Lorenz, Patrick Esser, and Björn Ommer. High-resolution image synthesis with latent diffusion models. In *Proc. IEEE Conf. Comp. Vis. Patt. Recogn.*, pages 10684–10695, 2022.
- [39] Yuming Jiang, Shuai Yang, Haonan Qiu, Wayne Wu, Chen Change

- Loy, and Ziwei Liu. Text2human: Text-driven controllable human image generation. *ACM Trans. Graphics*, 41(4):1–11, 2022.
- [40] Xuan Ju, Ailing Zeng, Chenchen Zhao, Jianan Wang, Lei Zhang, and Qiang Xu. Humansd: A native skeleton-guided diffusion model for human image generation. *arXiv preprint arXiv:2304.04269*, 2023.
- [41] Xian Liu, Jian Ren, Aliaksandr Siarohin, Ivan Skorokhodov, Yanyu Li, Dahua Lin, Xihui Liu, Ziwei Liu, and Sergey Tulyakov. Hyper-human: Hyper-realistic human generation with latent structural diffusion. *arXiv preprint arXiv:2310.08579*, 2023.
- [42] Shekoofeh Azizi, Simon Kornblith, Chitwan Saharia, Mohammad Norouzi, and David J Fleet. Synthetic data from diffusion models improves imagenet classification. *arXiv preprint arXiv:2304.08466*, 2023.
- [43] Roy Voetman, Maya Aghaei, and Klaas Dijkstra. The big data myth: Using diffusion models for dataset generation to train deep detection models. *arXiv preprint arXiv:2306.09762*, 2023.
- [44] Yonglong Tian, Lijie Fan, Phillip Isola, Huiwen Chang, and Dilip Krishnan. Stablerep: Synthetic images from text-to-image models make strong visual representation learners. *arXiv preprint arXiv:2306.00984*, 2023.
- [45] Weijia Wu, Yuzhong Zhao, Hao Chen, Yuchao Gu, Rui Zhao, Yefei He, Hong Zhou, Mike Zheng Shou, and Chunhua Shen. Datasetdm: Synthesizing data with perception annotations using diffusion models. *arXiv: Comp. Res. Repository*, 2023.
- [46] Olaf Ronneberger, Philipp Fischer, and Thomas Brox. U-net: Convolutional networks for biomedical image segmentation. In *Medical Image Computing and Computer-Assisted Intervention—MICCAI 2015: 18th International Conference, Munich, Germany, October 5–9, 2015, Proceedings, Part III* 18, pages 234–241. Springer, 2015.
- [47] Jonathan Ho, Ajay Jain, and Pieter Abbeel. Denoising diffusion probabilistic models. In H. Larochelle, M. Ranzato, R. Hadsell, M.F. Balcan, and H. Lin, editors, *NIPS*, volume 33, pages 6840–6851. Curran Associates, Inc., 2020.
- [48] Jiaming Song, Chenlin Meng, and Stefano Ermon. Denoising diffusion implicit models. *arXiv:2010.02502*, October 2020.
- [49] Christoph Schuhmann, Romain Beaumont, Richard Vencu, Cade Gordon, Ross Wightman, Mehdi Cherti, Theo Coombes, Aarush Katta, Clayton Mullis, Mitchell Wortsman, Patrick Schramowski, Srivatsa Kundurthy, Katherine Crowson, Ludwig Schmidt, Robert Kaczmarczyk, and Jenia Jitsev. Laion-5b: An open large-scale dataset for training next generation image-text models, 2022.
- [50] Minwoo Byeon, Beomhee Park, Haechon Kim, Sungjun Lee, Woonyuk Baek, and Saehoon Kim. Coyo-700m: Image-text pair dataset. <https://github.com/kakaobrain/coyo-dataset>, 2022.
- [51] Yuxin Fang, Bencheng Liao, Xinggang Wang, Jiemin Fang, Jiyang Qi, Rui Wu, Jianwei Niu, and Wenyu Liu. You only look at one sequence: Rethinking transformer in vision through object detection. In *Proc. Advances in Neural Inf. Process. Syst.*, 2021.
- [52] Lihe Yang, Bingyi Kang, Zilong Huang, Zhen Zhao, Xiaogang Xu, Jiashi Feng, and Hengshuang Zhao. Depth anything v2. *arXiv:2406.09414*, 2024.
- [53] Gwangbin Bae and Andrew J. Davison. Rethinking inductive biases for surface normal estimation. In *IEEE/CVF Conference on Computer Vision and Pattern Recognition (CVPR)*, 2024.
- [54] Zhendong Yang, Ailing Zeng, Chun Yuan, and Yu Li. Effective whole-body pose estimation with two-stages distillation. In *Proceedings of the IEEE/CVF International Conference on Computer Vision*, pages 4210–4220, 2023.
- [55] *Renderpeople*, 2022. <https://renderpeople.com>.
- [56] Wenjia Wang, Yongtao Ge, Haiyi Mei, Zhongang Cai, Qingping Sun, Yanjun Wang, Chunhua Shen, Lei Yang, and Taku Komura. Zolly: Zoom focal length correctly for perspective-distorted human mesh reconstruction. *arXiv preprint arXiv:2303.13796*, 2023.
- [57] Chandan Yeshwanth, Yueh-Cheng Liu, Matthias Nießner, and Angela Dai. Scannet++: A high-fidelity dataset of 3d indoor scenes. In *Proceedings of the IEEE/CVF International Conference on Computer Vision*, pages 12–22, 2023.
- [58] Donald Meagher. Geometric modeling using octree encoding. *Computer graphics and image processing*, 19(2):129–147, 1982.
- [59] OpenAI. Gpt-3: Generative pre-trained transformer 3. <https://openai.com/research/gpt-3>, 2020.
- [60] Hugo Touvron, Thibaut Lavril, Gautier Izacard, Xavier Martinet, Marie-Anne Lachaux, Timothée Lacroix, Baptiste Rozière, Naman Goyal, Eric Hambro, Faisal Azhar, et al. Llama: Open and efficient foundation language models. *arXiv preprint arXiv:2302.13971*, 2023.
- [61] Tao Jiang, Peng Lu, Li Zhang, Ningsheng Ma, Rui Han, Chengqi Lyu, Yining Li, and Kai Chen. Rtmpose: Real-time multi-person pose estimation based on mmpose, 2023.
- [62] Xiaoxuan Ma, Jiajun Su, Chunyu Wang, Wentao Zhu, and Yizhou Wang. 3d human mesh estimation from virtual markers. In *Proceedings of the IEEE/CVF Conference on Computer Vision and Pattern Recognition (CVPR)*, pages 534–543, June 2023.
- [63] huggingface. Sdxl-controlnet: Depth, 2023.
- [64] Weihang Wang, Qingsong Lv, Wenmeng Yu, Wenyi Hong, Ji Qi, Yan Wang, Junhui Ji, Zhuoyi Yang, Lei Zhao, Xixuan Song, Jiazheng Xu, Bin Xu, Juanzi Li, Yuxiao Dong, Ming Ding, and Jie Tang. Cogvlm: Visual expert for pretrained language models, 2023.
- [65] Martin Heusel, Hubert Ramsauer, Thomas Unterthiner, Bernhard Nessler, and Sepp Hochreiter. Gans trained by a two time-scale update rule converge to a local nash equilibrium. *Advances in neural information processing systems*, 30, 2017.
- [66] Mikolaj Bińkowski, Danica J Sutherland, Michael Arbel, and Arthur Gretton. Demystifying mmd gans. *arXiv preprint arXiv:1801.01401*, 2018.
- [67] Siwei Zhang, Qianli Ma, Yan Zhang, Zhiyin Qian, Taein Kwon, Marc Pollefeys, Federica Bogo, and Siyu Tang. Egobody: Human body shape and motion of interacting people from head-mounted devices. In *Proc. Eur. Conf. Comp. Vis.*, pages 180–200. Springer, 2022.
- [68] Chun-Hao P Huang, Hongwei Yi, Markus Höschle, Matvey Safroshkin, Tsvetelina Alexiadis, Senya Polikovskiy, Daniel Scharstein, and Michael J Black. Capturing and inferring dense full-body human-scene contact. In *Proc. IEEE Conf. Comp. Vis. Patt. Recogn.*, pages 13274–13285, 2022.
- [69] Akash Sengupta, Ignas Budvytis, and Roberto Cipolla. Synthetic training for accurate 3d human pose and shape estimation in the wild. *arXiv preprint arXiv:2009.10013*, 2020.
- [70] Ke Sun, Bin Xiao, Dong Liu, and Jingdong Wang. Deep high-resolution representation learning for human pose estimation. In *Proc. IEEE Conf. Comp. Vis. Patt. Recogn.*, pages 5693–5703, 2019.
- [71] thibaud. Sdxl-controlnet: Pose, 2023.
- [72] Hui En Pang, Zhongang Cai, Lei Yang, Tianwei Zhang, and Ziwei Liu. Benchmarking and analyzing 3d human pose and shape estimation beyond algorithms. In *Proc. Advances in Neural Inf. Process. Syst.*, 2022.
- [73] Muhammed Kocabas, Chun-Hao P Huang, Otmar Hilliges, and Michael J Black. Pare: Part attention regressor for 3d human body estimation. In *Proc. IEEE Int. Conf. Comp. Vis.*, pages 11127–11137, 2021.
- [74] Jing Lin, Ailing Zeng, Haoqian Wang, Lei Zhang, and Yu Li. One-stage 3d whole-body mesh recovery with component aware transformer. In *Proceedings of the IEEE/CVF Conference on Computer Vision and Pattern Recognition*, pages 21159–21168, 2023.
- [75] Nikos Kolotouros, Georgios Pavlakos, Michael J Black, and Kostas Daniilidis. Learning to reconstruct 3d human pose and shape via model-fitting in the loop. In *Proc. IEEE Int. Conf. Comp. Vis.*, pages 2252–2261, 2019.
- [76] Muhammed Kocabas, Chun-Hao P Huang, Joachim Tesch, Lea Müller, Otmar Hilliges, and Michael J Black. Spec: Seeing people in the wild with an estimated camera. In *Proc. IEEE Int. Conf. Comp. Vis.*, pages 11035–11045, 2021.
- [77] Kaiming He, Xiangyu Zhang, Shaoqing Ren, and Jian Sun. Deep residual learning for image recognition. In *Proc. IEEE Conf. Comp. Vis. Patt. Recogn.*, pages 770–778, 2016.
- [78] Gyeongsik Moon, Hongsuk Choi, and Kyoung Mu Lee. Accurate 3d hand pose estimation for whole-body 3d human mesh estimation. In *Proc. IEEE Conf. Comp. Vis. Patt. Recogn.*, pages 2308–2317, 2022.
- [79] Hongwen Zhang, Yating Tian, Yuxiang Zhang, Mengcheng Li, Liang An, Zhenan Sun, and Yebin Liu. Pymaf-x: Towards well-aligned full-body model regression from monocular images. *arXiv preprint arXiv:2207.06400*, 2022.
- [80] Chaorui Deng, Deyao Zhu, Kunchang Li, Chenhui Gou, Feng Li, Zeyu Wang, Shu Zhong, Weihao Yu, Xiaonan Nie, Ziang Song, Guang Shi, and Haoqi Fan. Emerging properties in unified multimodal pretraining. *arXiv preprint arXiv:2505.14683*, 2025.
- [81] Black Forest Labs, Stephen Batifol, Andreas Blattmann, Frederic Boesel, Saksham Consul, Cyril Diagne, Tim Dockhorn, Jack English, Zion English, Patrick Esser, Sumith Kulal, Kyle Lacey, Yam Levi, Cheng Li, Dominik Lorenz, Jonas Müller, Dustin Podell, Robin Rombach, Harry Saini, Axel Sauer, and Luke Smith. Flux.1 kontext: Flow matching for in-context image generation and editing in latent space, 2025.

- [82] Diederik P Kingma and Jimmy Ba. Adam: A method for stochastic optimization. *arXiv: Comp. Res. Repository*, 2014.
- [83] Yifei Yin, Chen Guo, Manuel Kaufmann, Juan Zarate, Jie Song, and Otmar Hilliges. Hi4d: 4d instance segmentation of close human interaction. In *Proc. IEEE Conf. Comp. Vis. Patt. Recogn.*, 2023.
- [84] Mihai Fieraru, Mihai Zanfir, Elisabeta Oneata, Alin-Ionut Popa, Vlad Olaru, and Cristian Sminchisescu. Three-dimensional reconstruction of human interactions. In *Proc. IEEE Conf. Comp. Vis. Patt. Recogn.*, June 2020.
- [85] OpenAI. Gpt-4 technical report, 2023.

## APPENDIX A

### A.1 Implement Details for Training ControlNet

HumanWild employs a customized multi-condition ControlNet to generate human images and corresponding annotations. In the preliminary phase of our research, we adopt the off-the-shelf depth-to-image ControlNet, and keypoint-to-image ControlNet, which are trained on the LAION5B dataset without filtering low-quality images. Experiments show that the pre-trained models face challenges when it comes to generating human images with hard poses. To resolve this issue, we collect high-quality human images from multiple datasets and then conduct finetuning on the collected datasets for better generation performance. We train the customized ControlNet with AdamW [82] in  $1e-5$  learning rate, and 0.01 weight decay for 80,000 iterations on 8 A100 GPUs. For training efficiency, we utilize Fully Sharded Data Parallel (FSDP) with ZeRO Stage 2, gradient checkpointing, and mixed-precision training



Fig. 9: Utilizing identical surface normal maps and control scale factor of the surface normal as input, we change the input text prompts.



Fig. 10: Utilizing identical surface normal maps and text prompts as input, we manipulate the control scale factor of the surface normal map across values of 0.75, 0.5, and 0.25, respectively.

## APPENDIX B

### B.1 Failure Cases of the Off-the-shelf ControlNet

In Fig. 11, we show some failure cases of the data pairs generated by off-the-shelf ControlNet trained on general datasets. The inconsistency of the image and 3D mesh would affect the performance of the 3D human pose estimation. Thus, it is necessary to retrain a customized multi-condition





Fig. 11: Failure cases of the data pairs generated by general ControlNet. See highlighted regions with red circles.

ControlNet with the human-centric dataset collected in this work.

## B.2 More Visualization of Generated Data Sample

We show more data sample visualization with diverse scenes and body shapes in Fig. 12.

We show visualization results on human interactions in Fig. 13, which demonstrates that our pipeline can generate well-aligned image-annotation pairs where people are with close interactions. The generated data pairs are of great value in enhancing existing human interaction datasets collected in the studio environment. (*e.g.*, Hi4D [83] and CHI3D [84])

## B.3 Text Prompt Examples Generated by LLM

In Table 10, we show some text prompt examples, which are generated by ChatGPT [85] with diverse human actions and scenes.

TABLE 10: Text prompt examples.

gender	action	environment
a man	playing soccer	at the park
a woman	swimming	in the pool
a man	shopping	at the mall
a woman	running	in the park
a man	studying	at the library
a man	working	at the office
a man	chatting	at a cafe

## B.4 Misalignment Analysis of Complicated Prompts and Spatial Conditions

We present instances of failure where text prompts conflict with the spatial condition, *e.g.*, surface normal. Specifically, when the text prompt suggests an action that deviates from the surface normal map, the resulting images often fail to adhere to the text prompt, particularly when the control factor of the surface normal map approaches 1.0. As shown in Fig. 9, despite employing the same input surface normal map and a control factor of 0.95, the generated images exhibit similar foreground human identities but differ in background elements corresponding to distinct text prompts. Fig. 10 illustrates that when the control factor of the surface normal is extremely low, the generated images may disregard the surface normal map condition.



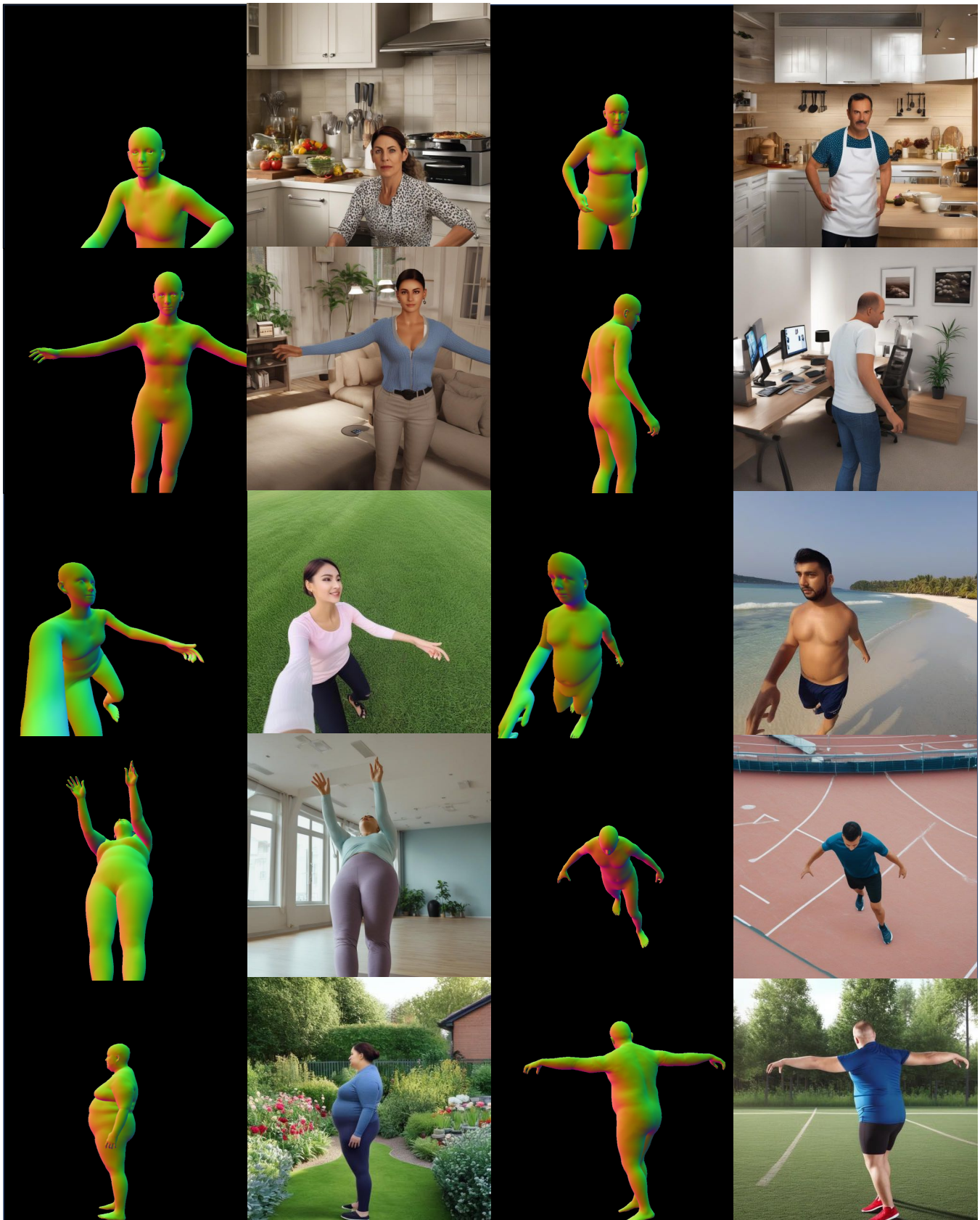


Fig. 12: More Data sample visualization of HumanWild. For each data sample, the left side is the normal image rendered from SMPL-X model, the right side is the image generated by HumanWild pipeline. The first two rows demonstrate the indoor activities. The third row shows the generated images with huge distortion. The fourth row describes the diverse camera views. The fifth row shows overweight human bodies.





Fig. 13: Visualization of Human interaction. The SMPL interaction annotations are sampled from the Hi4D [83] dataset.